This work was written as part of one of the author's official duties as an Employee of the United States Government and is therefore a work of the United States Government. In accordance with 17 U.S.C. 105, no copyright protection is available for such works under U.S. Law. Access to this work was provided by the University of Maryland, Baltimore County (UMBC) ScholarWorks@UMBC digital repository on the Maryland Shared Open Access (MD-SOAR) platform.

Please provide feedback

Please support the ScholarWorks@UMBC repository by emailing scholarworks-group@umbc.edu and telling us what having access to this work means to you and why it's important to you. Thank you.

The Astronomical Journal, 128:1570–1587, 2004 October
© 2004. The American Astronomical Society. All rights reserved. Printed in U.S.A.

# VLBA SNAPSHOT IMAGING SURVEY OF SCINTILLATING SOURCES

Roopesh Ojha
Australia Telescope National Facility, CSIRO, P.O. Box 76, Epping, NSW 1710, Australia; rojha@atnf.csiro.au

Alan L. Fey
United States Naval Observatory, 3450 Massachusetts Avenue, NW, Washington, DC 20392-5420

James E. J. Lovell and David L. Jauncey
Australia Telescope National Facility, CSIRO, c/o Research School of Astronomy and Astrophysics, Mount Stromlo Observatory, Cotter Road, Weston Creek, ACT 2611, Australia

and

Kenneth J. Johnston
United States Naval Observatory, 3450 Massachusetts Avenue, NW, Washington, DC 20392-5420
*Received 2004 March 12; accepted 2004 July 1*

## ABSTRACT

We present 8.4 GHz Very Long Baseline Array (VLBA) observations of 75 extragalactic radio sources drawn from the scintillating sources discovered in the Microarcsecond Scintillation-induced Variability survey. This survey clearly showed that the fraction of scintillating sources and the amplitude of their variability increases strongly with decreasing flux density, raising the possibility that scintillating sources may be systematically extremely core dominated. The observations presented here were designed to investigate this hypothesis. The results indeed show that most of the scintillating sources we observed with the VLBA have an extremely compact, core-dominated morphology, which has important implications for interpretations of the scintillation seen in these sources. In addition, these sources are potential candidates for inclusion in the International Celestial Reference Frame.

*Key words:* galaxies: active — galaxies: jets — galaxies: nuclei — polarization — quasars: general — reference systems

*Online material:* machine-readable tables

## 1. INTRODUCTION

It is now clear that interstellar scintillation (ISS; e.g., Rickett 1990) is the principal cause of rapid variations in flux density seen in some compact, flat-spectrum radio sources at centimeter wavelengths (Jauncey et al. 2003a; Wagner & Witzel 1995). One predicted effect of ISS is a time delay in the variability pattern arrival times at two widely separated telescopes. Time delays of minutes have been observed for several of the most rapidly variable sources (Bignall et al. 2003; Dennett-Thorpe & de Bruyn 2002). In addition, an annual cycle in the characteristic timescale of the variability has now been found in at least five sources (Rickett et al. 2001; Jauncey et al. 2003b; Jauncey & Macquart 2001; Dennett-Thorpe & de Bruyn 2001; Bignall et al. 2002). Such an annual cycle results from the changing relative velocity of the interstellar medium (ISM) seen from Earth as it moves around the Sun. For such observations, ISS is the only plausible explanation.

The Microarcsecond Scintillation-induced Variability (MASIV) survey (Lovell et al. 2003) aims to construct a sample of 100 to 150 scintillating extragalactic sources with which to examine both the microarcsecond structure and the parent population of these sources, as well as to probe the turbulent ISM responsible for the scintillation. A total of 710 compact, flat-spectrum sources distributed over the northern sky were surveyed using the Very Large Array (VLA) at a frequency of 4.9 GHz. Over 100 new scintillating radio sources, with variability timescales from hours to days, have already been discovered by this program. However, rapid, large-amplitude variables such as J1819+3845 (Dennett-Thorpe & de Bruyn 2002) are rare.

The MASIV VLA survey results showed an increase in the fraction of highly variable scintillators (those with rms flux density variations above 4%) with decreasing flux density. They also showed an increase in their amplitude of variability with decreasing flux density. These results raised the possibility that the milliarcsecond scale structures of scintillators may differ from that of nonscintillators in that the weaker sources are more "core dominated," or rather, less milliarcsecond "jet" dominated. Thus, low flux density scintillating sources may form a distinct population with a differing morphology.

To investigate this possibility, we have used the National Radio Astronomy Observatory's (NRAO)[1] Very Long Baseline Array (VLBA) to image the milliarcsecond-scale structure of 75 low flux density (see § 2) scintillators discovered in the MASIV survey. Section 2 describes our sample, experimental parameters, and data reduction. In § 3 we present the images in both total intensity and linearly polarized flux density and tabulate image parameters and the results of models fitted to each observed source. We also present distributions of source flux density and source compactness. In § 4 we discuss the potential use of low-flux scintillator sources, such as those

[1] The National Radio Astronomy Observatory is a facility of the National Science Foundation operated under cooperative agreement by Associated Universities, Inc.

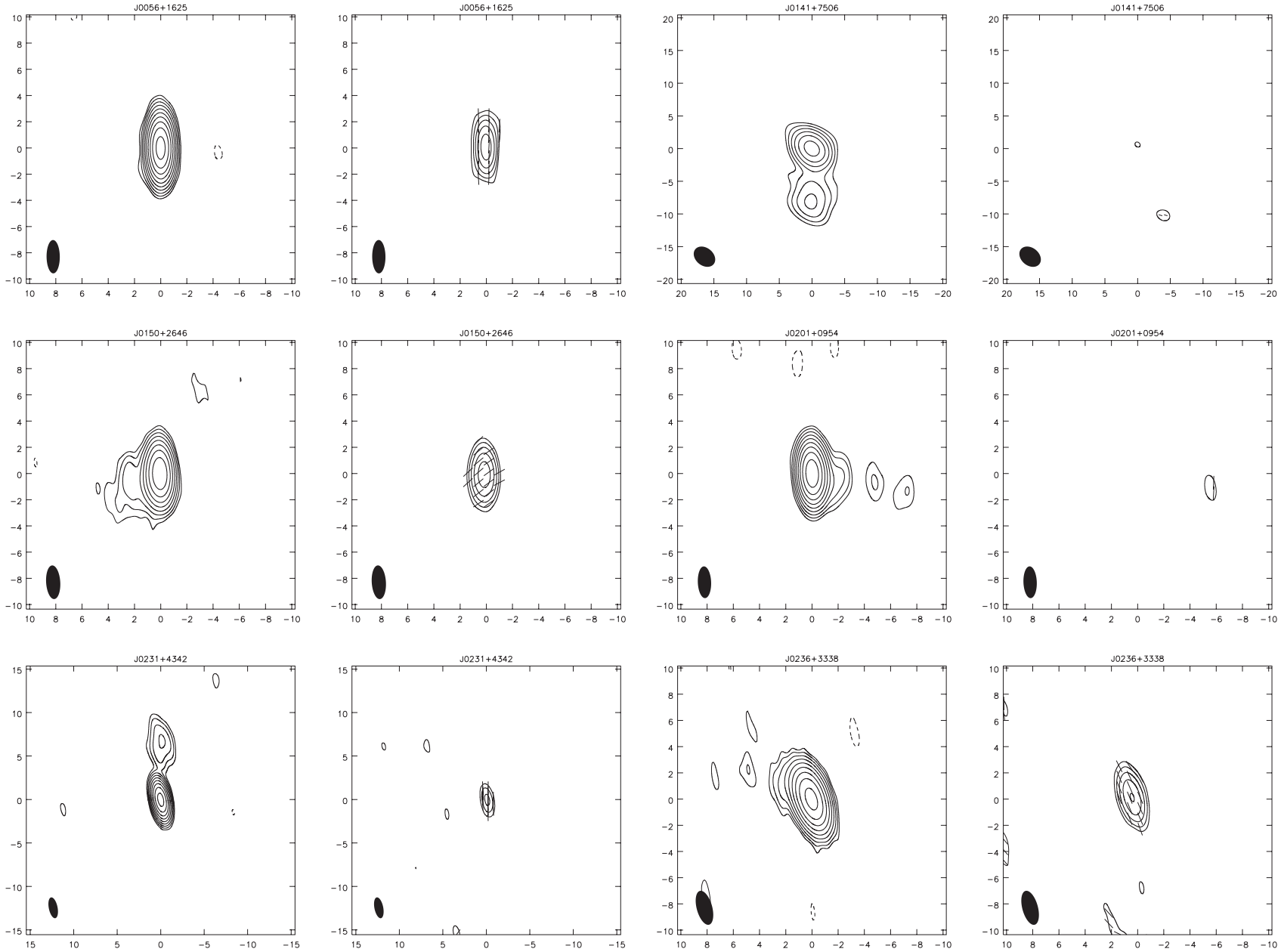


FIG. 1.—Total intensity and polarized intensity contour plots of 75 scintillating extragalactic radio sources at 8.4 GHz. Total intensity image parameters are listed in Table 1, and polarized intensity image parameters are listed in Table 2. The scale of each image is in milliarcseconds. The FWHM Gaussian restoring beam applied to the images is shown as a filled ellipse in the lower left of each panel. In the polarized images the contours indicate polarized intensity, and the tick marks indicate the direction of the inferred electric field component in the plane of the sky. The length and spacing of these tick marks have no significance.

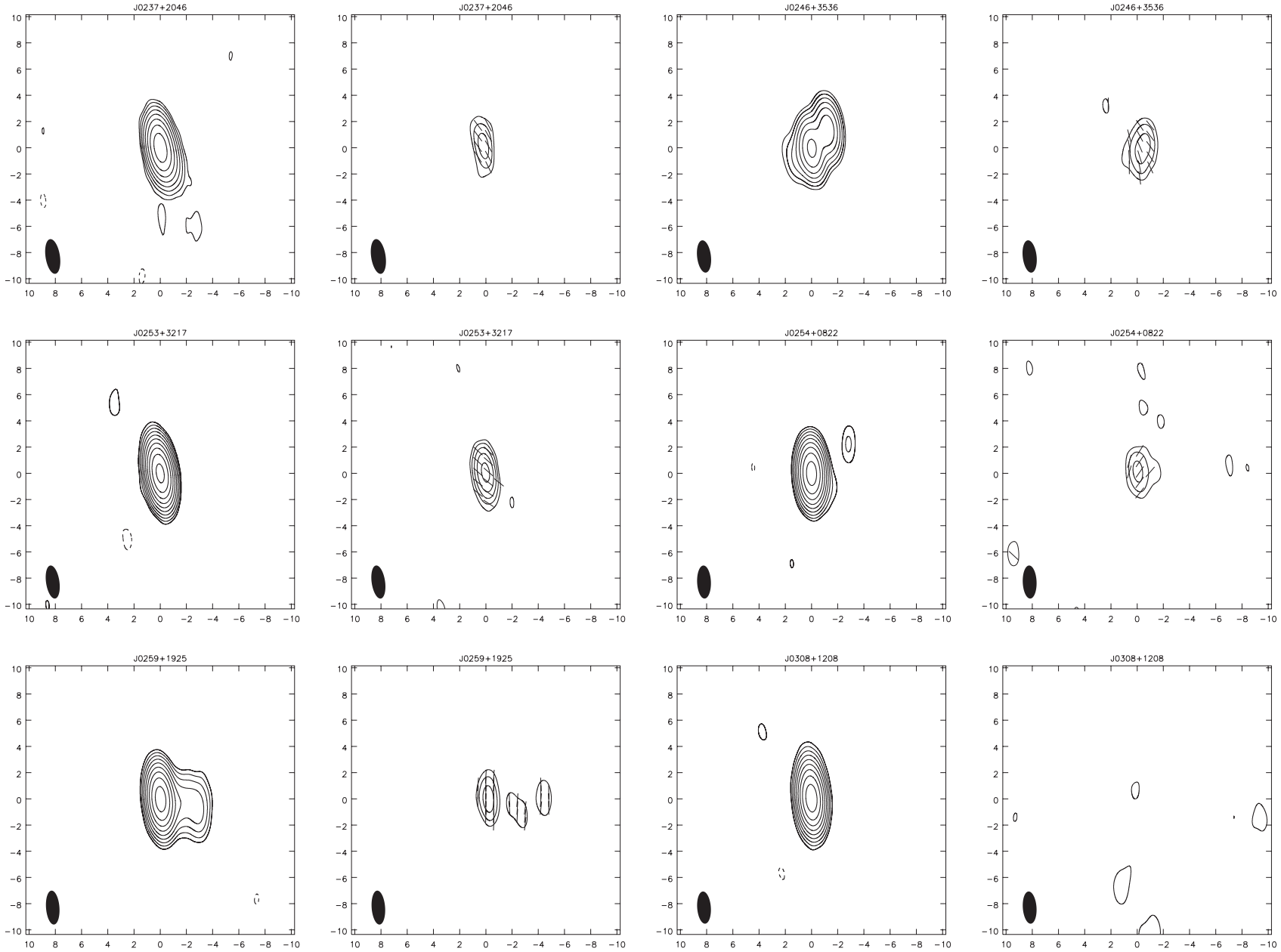


FIG. 1.—*Continued*

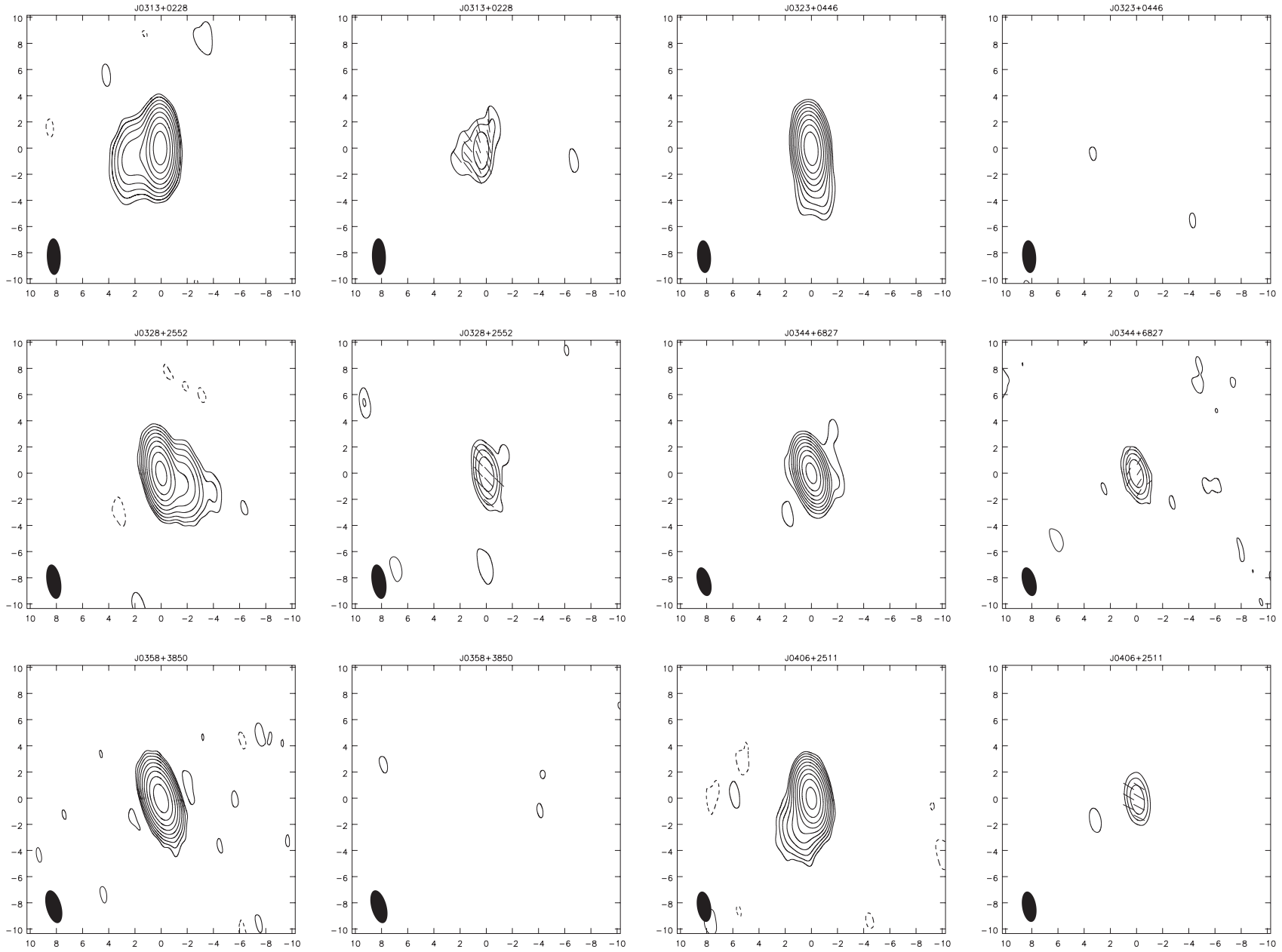


FIG. 1.—*Continued*

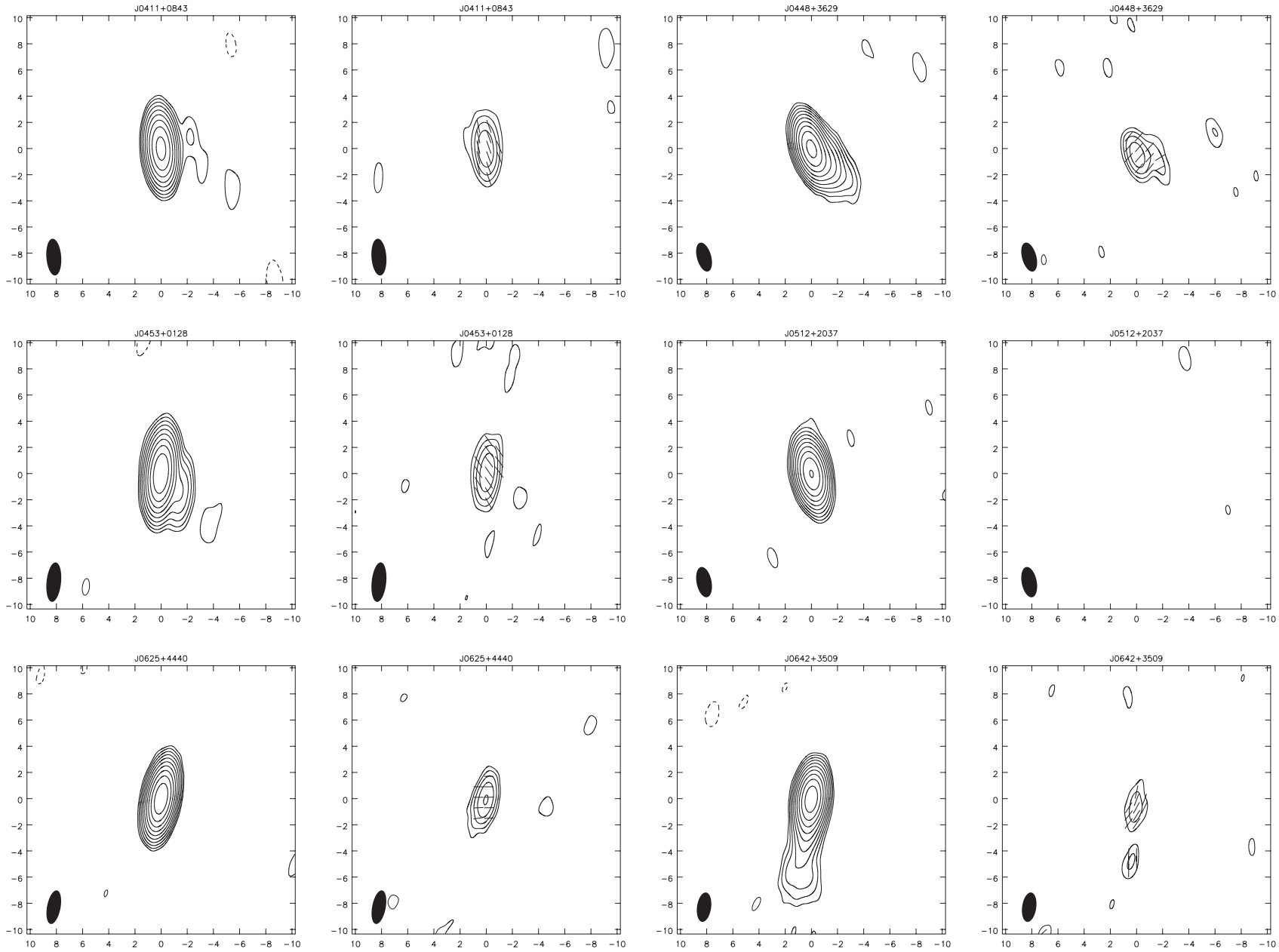


FIG. 1.—*Continued*

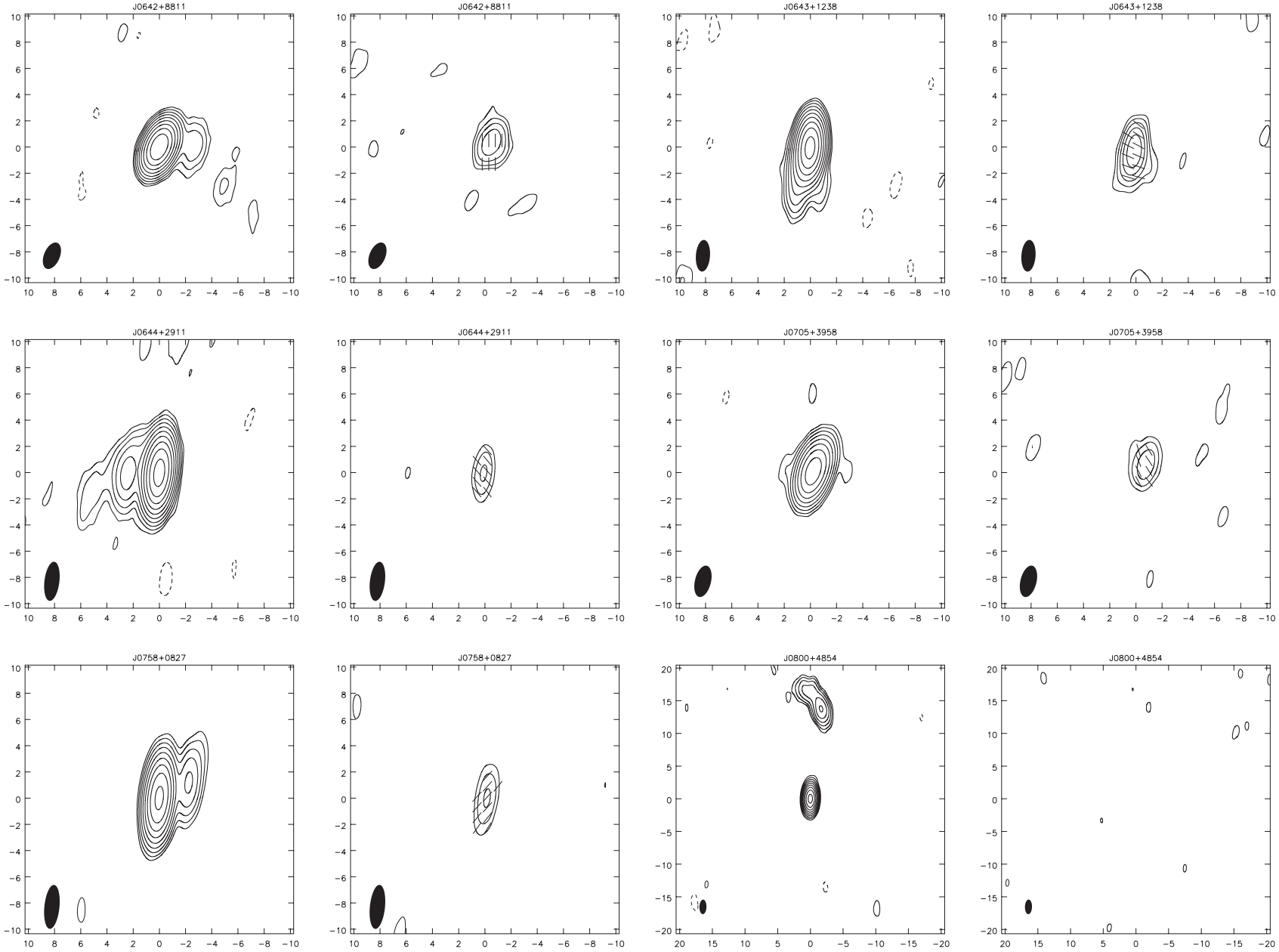


FIG. 1.—*Continued*

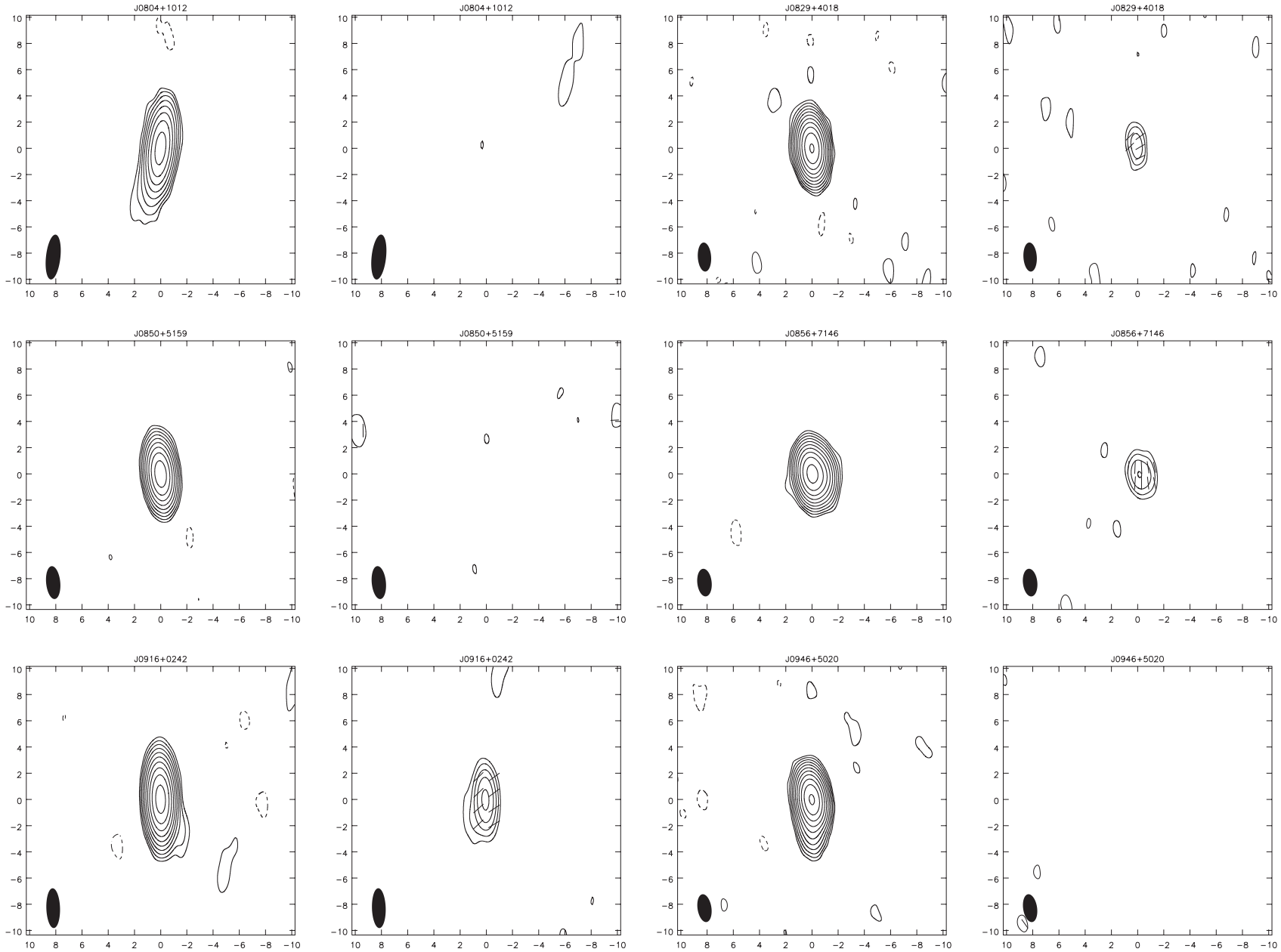


FIG. 1.—*Continued*

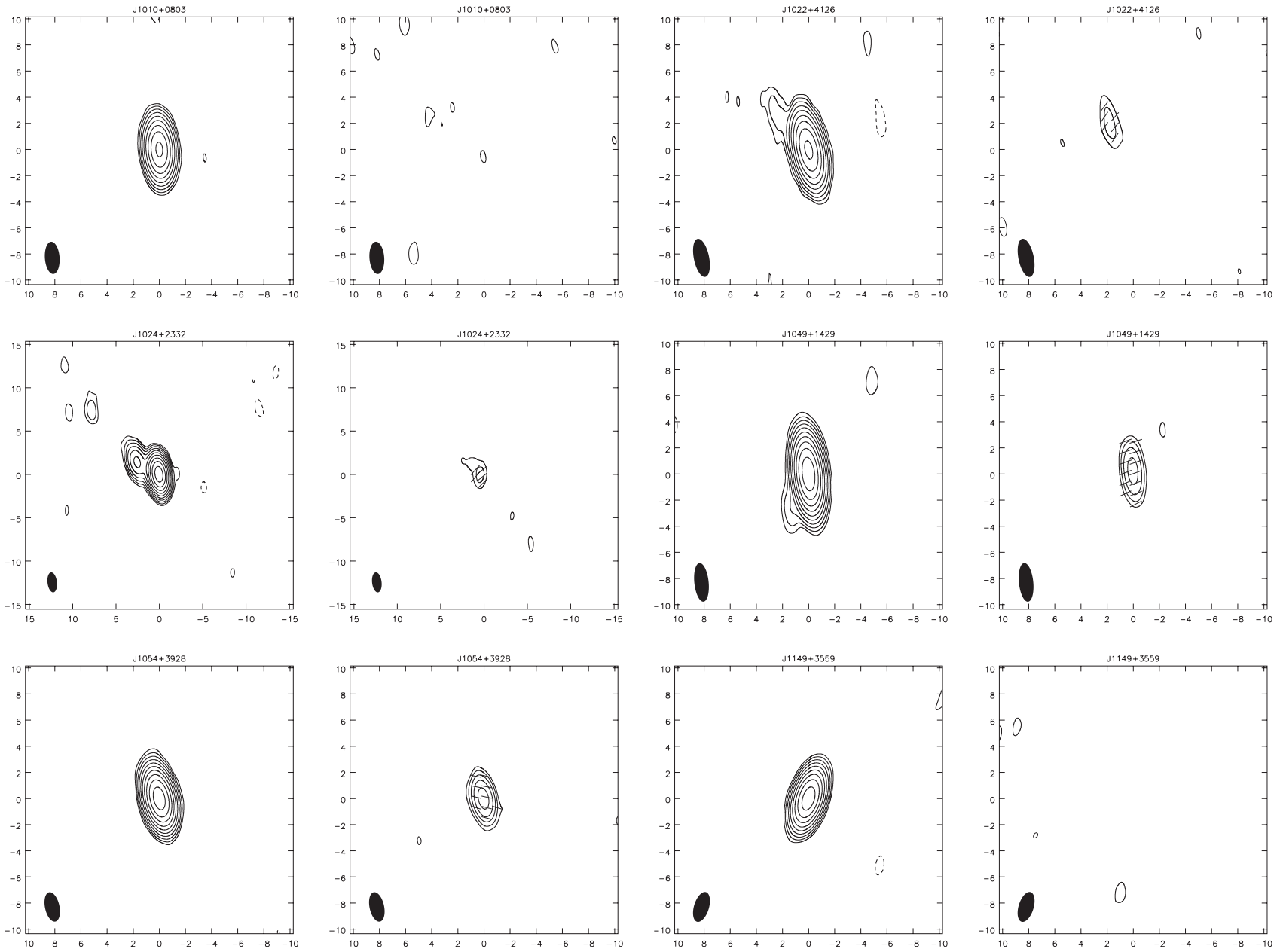


FIG. 1.—*Continued*

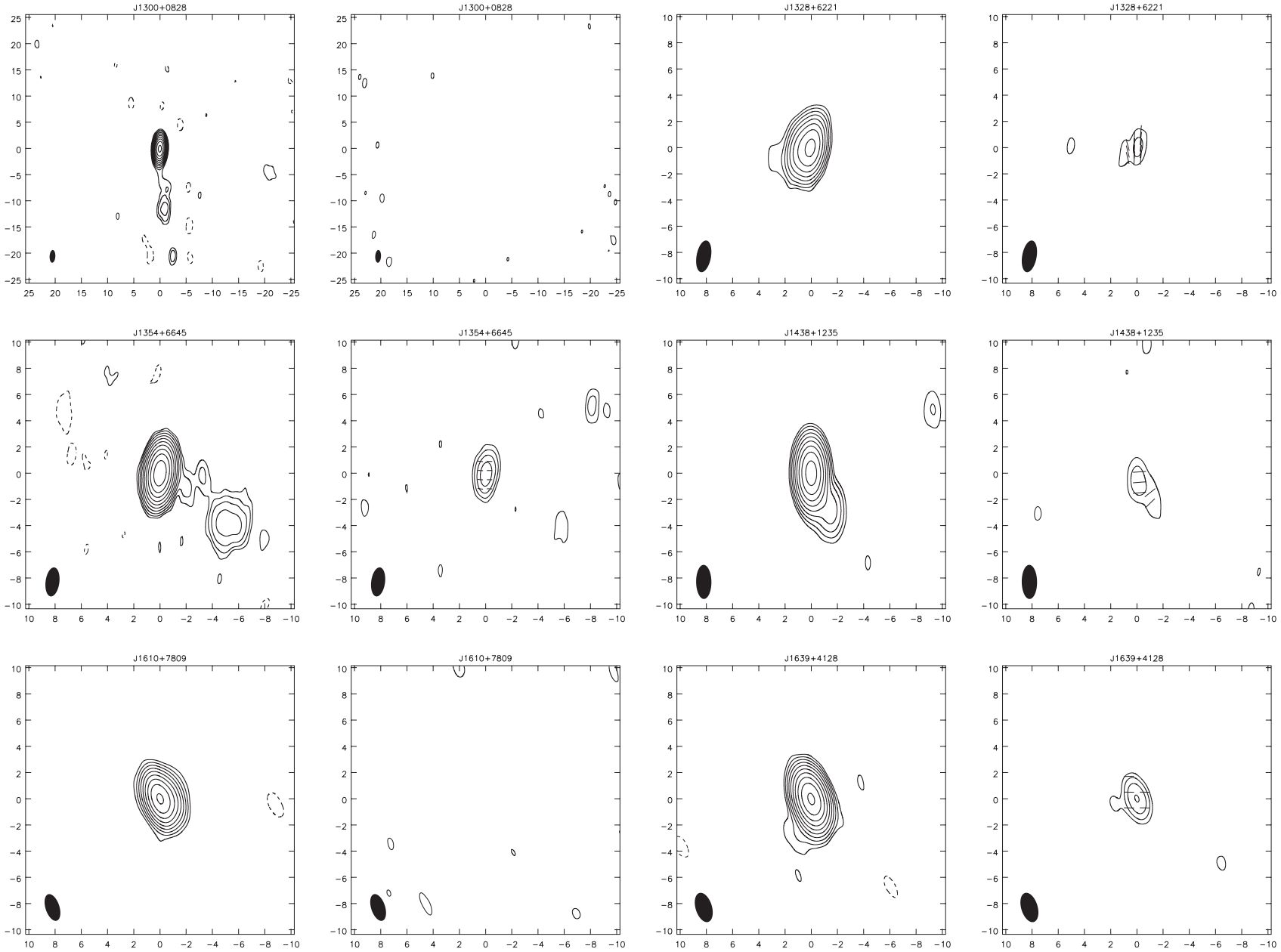


FIG. 1.—*Continued*

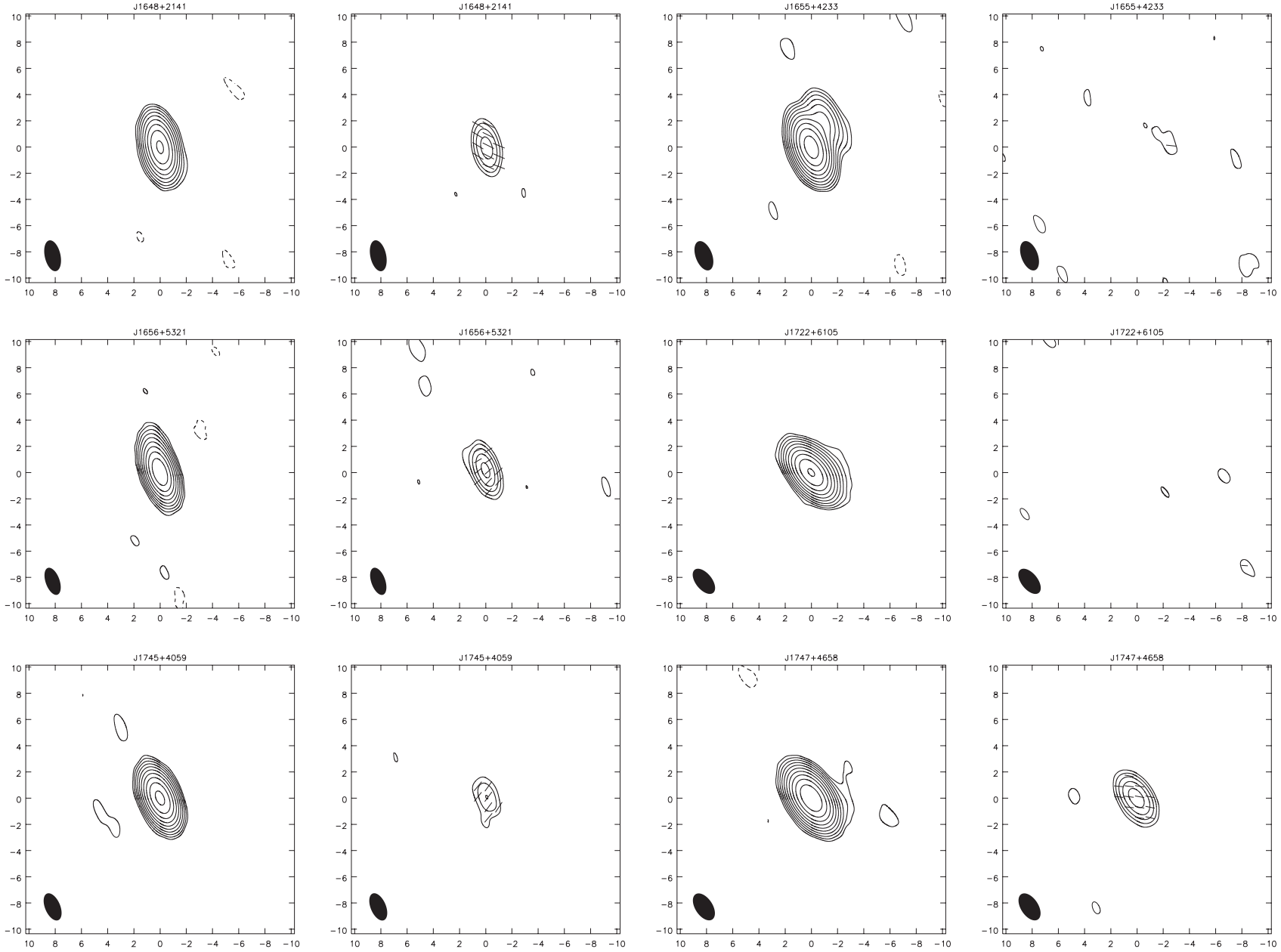


FIG. 1.—*Continued*

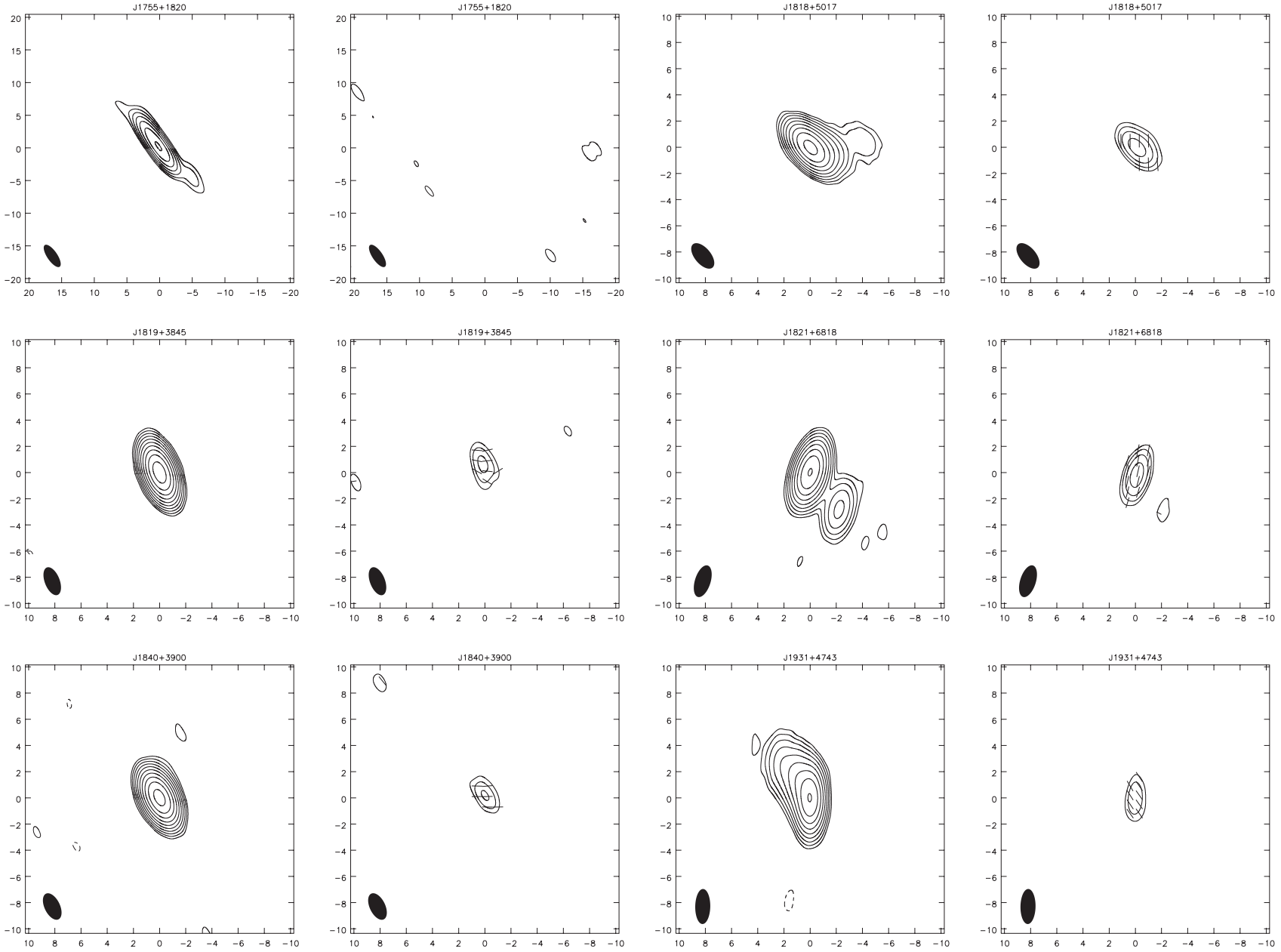


FIG. 1.—*Continued*

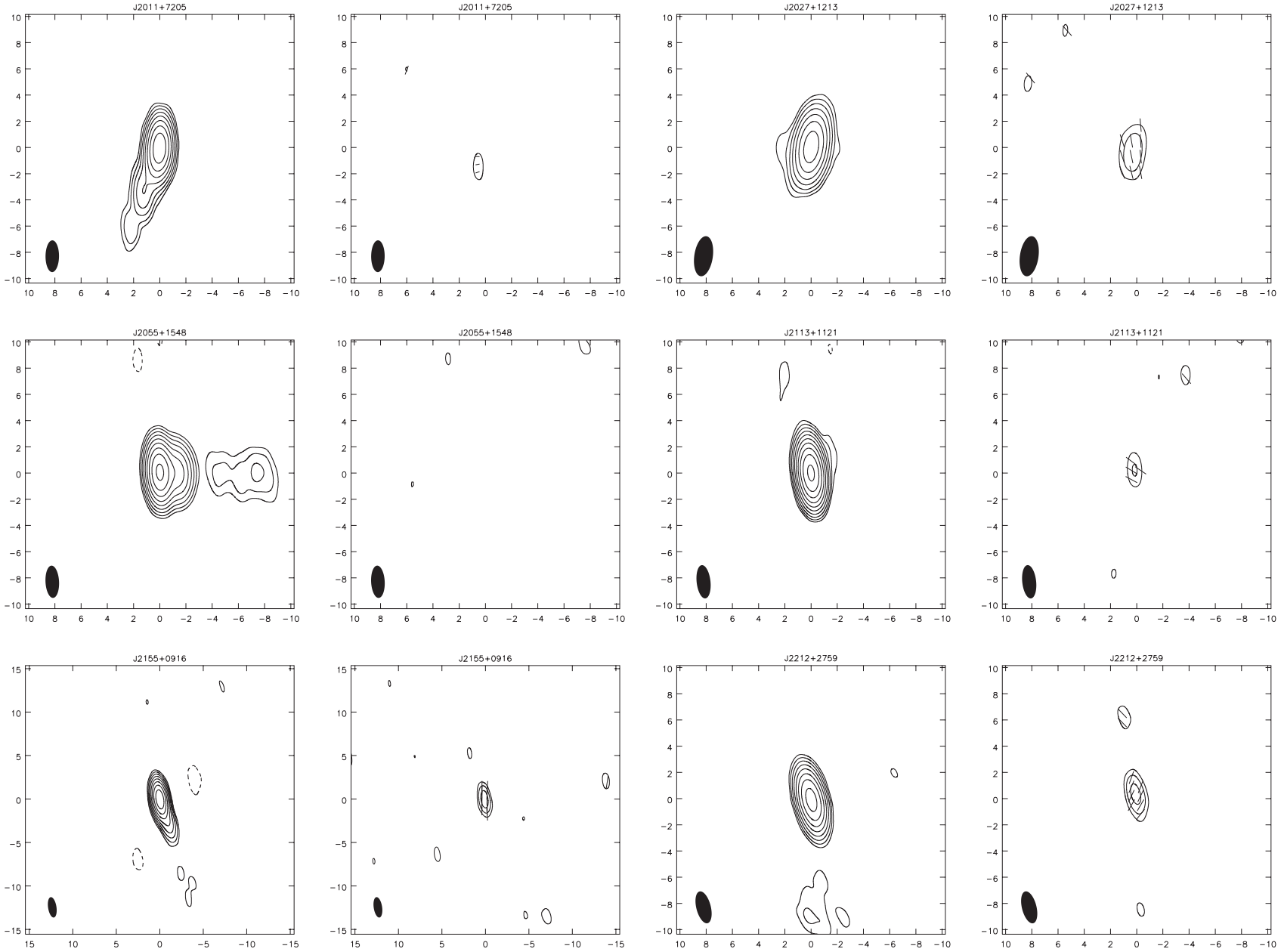


FIG. 1.—*Continued*

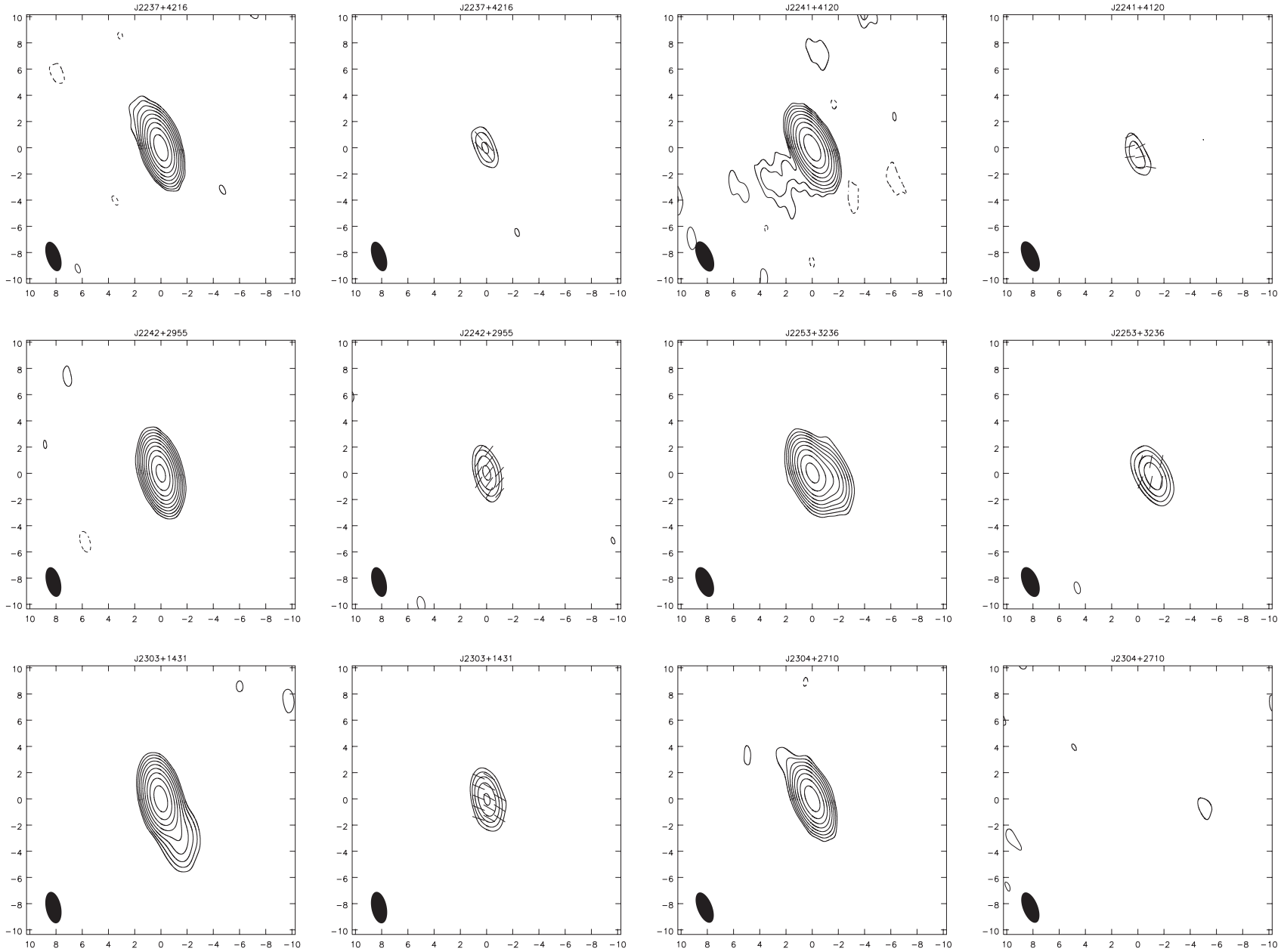


FIG. 1.—*Continued*

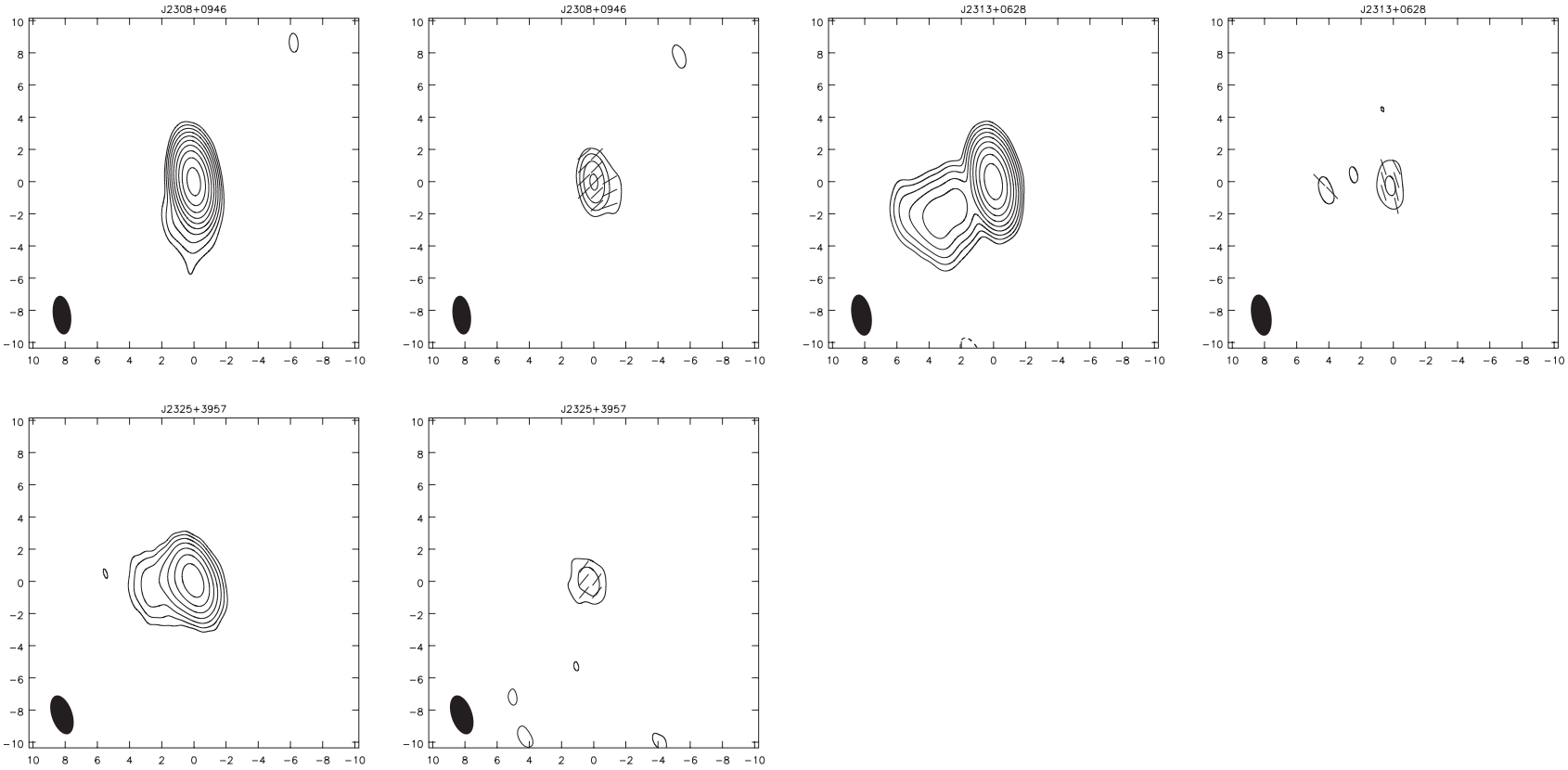


FIG. 1.—*Continued*

TABLE 1
PARAMETERS OF NATURALLY WEIGHTED TOTAL INTENSITY IMAGES

| SOURCE | BEAM[a] $a$ (mas) | $b$ (mas) | $\phi$ (deg) | PEAK (mJy beam$^{-1}$) | rms[b] (mJy beam$^{-1}$) | CONTOUR LEVELS[c] (mJy beam$^{-1}$) |
|---|---|---|---|---|---|---|
| J0056+1625..... | 2.5 | 1.0 | 1 | 259.98 | 0.12 | $0.37 \times (1, \ldots, 2^9)$ |
| J0141+7506..... | 3.6 | 2.7 | 51 | 39.47 | 0.29 | $0.87 \times (1, \ldots, 2^5)$ |
| J0150+2646..... | 2.6 | 1.1 | 4 | 87.70 | 0.12 | $0.37 \times (1, \ldots, 2^7)$ |
| J0201+0954..... | 2.4 | 1.0 | 2 | 77.78 | 0.06 | $0.18 \times (1, \ldots, 2^8)$ |
| J0231+4342..... | 2.4 | 1.0 | 12 | 72.36 | 0.07 | $0.21 \times (1, \ldots, 2^8)$ |

NOTE.—Table 1 is presented in its entirety in the electronic edition of the Astronomical Journal. A portion is shown here for guidance regarding its form and content.

[a] The restoring beam is an elliptical Gaussian with FWHM major axis $a$ and minor axis $b$, with the major axis in position angle $\phi$ (measured from north through east).

[b] The rms of the residuals of the final hybrid image.

[c] Contour levels are represented by the geometric series $1, \ldots, 2^n$; e.g., for $n = 5$ the contour levels would be $\pm 1$, 2, 4, 8, 16, and 32.

observed here, to expand and improve the International Celestial Reference Frame (ICRF), and our conclusions are set out in § 5. Comparison of the milliarcsecond-scale morphology in total intensity and linear polarization of this sample of scintillators with that of nonscintillators is the subject of future work.

## 2. OBSERVATIONS AND DATA REDUCTION

We used the VLBA to observe 75 sources during two 24 hr experiments on 2003 January 27 and 30. Our sources were all scintillators discovered by the MASIV survey (Lovell et al. 2003) and were selected according to the following criteria:

1. Point sources at the resolution of the VLA.
2. Spectral index from 1.4 to 4.9 GHz flatter than 0.5.
3. Flux density at 4.9 GHz less than 0.3 Jy.
4. rms flux density variations during a 72 hr period of $S_{\rm rms} > [0.003^2 + (0.02S)^2]^{1/2}$ Jy, where $S$ is the mean flux measured by MASIV at 4.9 GHz.
5. As evenly distributed in right ascension as possible, given the list of MASIV scintillator sources meeting the above criteria.

The observations were made at 8.417 GHz ($\lambda = 4$ cm, X band) with right- and left-circular polarizations recorded using 2 bit sampling at 128 Mbits s$^{-1}$ and a total bandwidth of 16 MHz. Two intermediate frequencies (IFs),[2] each divided into 16 channels of width 0.5 MHz, were used for right- and left-circular polarizations. Each source was observed for a total of 30 minutes with the observations split into four 7.5 minute long scans at widely spaced hour angles to ensure adequate $u$-$v$ plane coverage.

The data were correlated at the VLBA correlator in Socorro, New Mexico, and were loaded into NRAO's Astronomical Image Processing System (AIPS; Bridle & Greisen 1994; Greisen 1988). They were then calibrated using standard techniques for Very Long Baseline Interferometry (VLBI) polarization, e.g., Cotton (1993) and Roberts et al. (1994). After data inspection and initial editing, a correction was made for errors in the amplitudes in the cross-correlation spectrum that arise from errors in sampler thresholds, using measurements of the autocorrelation spectrum. Measurements of antenna gain and system temperatures were then used to derive the amplitude calibration for each antenna. The phase of the parallactic angle

[2] In this context "intermediate frequency" refers to a single signal path between a telescope and the correlator. Our total bandpass is divided into IFs that are adjacent in frequency. IFs should be distinguished from the narrow spectral channels into which they are subdivided, as the geometrical and propagation errors affecting the data can be large enough to cause significant phase changes across an IF bandwidth.

TABLE 2
PARAMETERS OF NATURALLY WEIGHTED LINEAR POLARIZATION IMAGES

| SOURCE | BEAM[a] $a$ (mas) | $b$ (mas) | $\phi$ (deg) | PEAK (mJy beam$^{-1}$) | rms[b] (mJy beam$^{-1}$) | CONTOUR LEVELS[c] (mJy beam$^{-1}$) |
|---|---|---|---|---|---|---|
| J0056+1625..... | 2.5 | 1.0 | 0 | 9.42 | 0.13 | $0.38 \times (1, \ldots, 2^4)$ |
| J0141+7506..... | 3.6 | 2.7 | 51 | 0.93 | 0.09 | 0.81 |
| J0150+2646..... | 2.6 | 1.1 | 4 | 9.19 | 0.13 | $0.39 \times (1, \ldots, 2^4)$ |
| J0201+0954..... | 2.4 | 1.0 | 2 | 0.43 | 0.04 | 0.24 |
| J0231+4342..... | 2.4 | 1.0 | 11 | 1.21 | 0.05 | $0.25 \times (1, \ldots, 2^2)$ |

NOTE.—Table 2 is presented in its entirety in the electronic edition of the Astronomical Journal. A portion is shown here for guidance regarding its form and content.

[a] The restoring beam is an elliptical Gaussian with FWHM major axis $a$ and minor axis $b$, with the major axis in position angle $\phi$ (measured from north through east).

[b] The rms of the residuals of the final hybrid image.

[c] Contour levels are represented by the geometric series $1, \ldots, 2^n$; e.g., for $n = 5$ the contour levels would be $\pm 1$, 2, 4, 8, 16, and 32. When $n = 0$, only the single contour level is given.

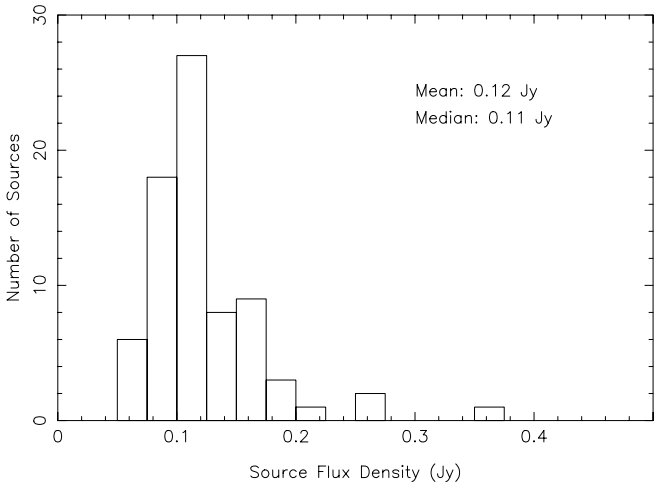


FIG. 2.—Distribution of the source flux density for the 75 observed scintillating extragalactic radio sources. The total flux density is defined as the total CLEANed flux density (i.e., the sum of all CLEAN components).

was removed from the residual phases, and the supplied pulse calibration information was then applied. Global fringe fitting was performed independently on each IF and polarization using an implementation of the Schwab & Cotton (1983) algorithm. Then a short (2 minute) section of cross-hand data from a strongly polarized calibrator was fringe-fitted to determine the multiband delay difference between the right- and left-hand systems of the array, and the resulting correction was applied to the rest of the data. Finally, the data were averaged across the channels within each IF and averaged over a 20 s time interval.

The effects of feed leakage terms (also known as instrumental terms or *D*-terms; these represent the percentage of nominally orthogonally polarized flux a feed receives) were calculated (Leppänen et al. 1995) on a strong source with simple total intensity structure, observed over a wide range in parallactic angle. Calibration of the absolute polarization position angle (also known as electric vector position angle [EVPA]) was performed using sources for which contemporaneous VLA observations were available from the VLA/VLBA Polarization Calibration Page.[3] The accuracy of this correction was confirmed by comparing results from multiple sources, which suggest the uncertainty in the EVPA calibration is $\sim 4^{\circ}$, with the variability in the EVPAs of the calibrator sources being the primary source of error (Taylor & Myers 2000).

After applying *D*-terms and EVPA corrections, further editing, self-calibration, and imaging of all sources was done using the Caltech DIFMAP package (Shepherd 1997; Shepherd et al. 1994) and AIPS. The final total intensity and polarized contour maps shown in Figure 1 were made using the AIPS++[4] software package.

## 3. RESULTS

The resulting total intensity and polarized intensity contour plots of 75 scintillating extragalactic radio sources observed with the VLBA at 8.4 GHz are shown in Figure 1. Tables 1 and 2 list parameters of the total intensity and polarized images, respectively. Following the source name, the next three columns list the major axis, minor axis, and position angle of the beam. The next two columns list the peak and rms flux density of the image. The final column indicates the contour levels used for each image. In the polarized intensity images the contours indicate polarized intensity, and the tick marks indicate the direction of the inferred electric field component in the plane of the sky. The length and spacing of these tick marks haves no significance.

The distribution of the source flux density (sum of all CLEAN components) is shown in Figure 2. Values range from a minimum of 50 mJy to a maximum of 370 mJy. The mean flux density is 120 mJy with a median of 110 mJy.

Gaussian models were fitted to the self-calibrated total intensity visibility data using the Caltech DIFMAP package. The results of the model fitting are listed in Table 3. After the source name the following items are listed: component number, total component flux, distance of component from core, orientation of component with respect to the core component, length of major axis of component, axial ratio of component (1 for circular component), and orientation of major axis of component. The distribution of fitted core angular size (in which the core is assumed to be the fitted component at the origin of the image) has a mean of 0.11 mas and a median of 0.10 mas. Nineteen sources have completely unresolved cores. The distribution of component angular radii from the core has a mean of 2.9 mas and a median of 2.1 mas. Only three

[3] Available at http://www.aoc.nrao.edu/~smyers/calibration.

[4] See http://aips2.nrao.edu.

TABLE 3
GAUSSIAN MODELS FITTED TO TOTAL INTENSITY IMAGES[a]

| Source | Component | $S$ (mJy) | $r$ (mas) | $\theta$ (deg) | $a$ (mas) | $b/a$ | $\phi$ (deg) |
|---|---|---|---|---|---|---|---|
| J0056+1625 | 1 | 260.6 | 0.0 | ... | 0.04 | 1.00 | ... |
| J0141+7506 | 1 | 43.3 | 0.0 | ... | 1.17 | 0.29 | −7 |
| | 2 | 7.6 | 4.9 | −175 | 3.63 | 1.00 | ... |
| | 3 | 13.1 | 8.4 | 179 | 2.49 | 1.00 | ... |
| J0150+2646 | 1 | 81.0 | 0.0 | ... | 0.12 | 1.00 | ... |
| | 2 | 16.3 | 0.7 | 124 | 0.13 | 1.00 | ... |
| | 3 | 5.3 | 2.5 | 112 | 1.42 | 1.00 | ... |

NOTE.—Table 3 is presented in its entirety in the electronic edition of the Astronomical Journal. A portion is shown here for guidance regarding its form and content.

[a] The models fitted to the visibility data are of Gaussian form with flux density $S$ and FWHM major axis $a$ and minor axis $b$, with the major axis in position angle $\phi$ (measured from north through east). Components are separated from the (arbitrary) origin of the image by an amount $r$ in position angle $\theta$, which is the position angle (measured from north through east) of a line joining the components with the origin.

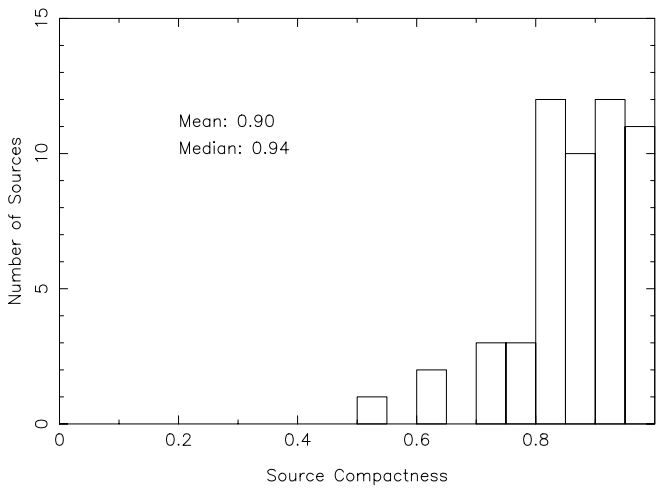


FIG. 3.—Distribution of source compactness (ratio of core flux density to total flux density) for the 75 observed scintillating extragalactic radio sources. The core flux density is defined as the sum of the CLEANed flux density within one synthesized beam. The total flux density is defined as the total CLEANed flux density (i.e., the sum of all CLEAN components).

components were found to be separated by greater than 10 mas from the core.

As an additional estimate of the compactness of the sources, we calculate the ratio of the core flux density to the total flux density. The core flux density is defined as the sum of the CLEANed flux density within one synthesized beam. The total flux density is defined as the total CLEANed flux density (i.e., the sum of all CLEAN components). The distribution of source compactness (ratio of core flux density to total flux density) is shown in Figure 3. With a mean value of 0.90 and a median of 0.94, Figure 3 indicates that scintillating extragalactic radio sources in this sample are extremely compact and core dominated. This result has important implications for interpretations of scintillation seen in compact radio sources. This will be explored in a future paper. The degree of compactness of these sources also suggests their efficacy as reference sources in future realizations of the radio reference frame as discussed below.

## 4. SCINTILLATING SOURCES AS ICRF SOURCES: VIABILITY AND BENEFITS

VLBI observations of selected strong compact extragalactic radio sources have been used to define and maintain a radio reference frame with submicroarcsecond precision (Ma et al. 1998). This International Celestial Reference Frame (ICRF) was adopted as the fundamental celestial reference frame at the 23rd General Assembly of the International Astronomical Union held on 1997 August 20 in Kyoto, Japan. The ICRF is currently defined by the radio positions of 212 extragalactic objects obtained using the technique of VLBI at radio frequencies of 2.3 and 8.4 GHz over the past 20 years.

The ICRF is currently limited by a number of factors. First, there is a deficit of defining sources, particularly in the southern hemisphere (although this is being addressed; e.g., Fey et al. 2004). Many defining sources have variable core-jet structure, which causes position variations, which can, in principle, be corrected. Finally, the ICRF is composed mostly of the brighter (>0.2 Jy at 8.4 GHz) sources, many of which suffer the most from structure problems. Thus, future improvement will involve both increasing the number of defining sources, as well as incorporating sources that have little or no structure, presumably leading to increased position stability.

The observations reported here show that low flux density scintillating sources are among the most compact, core-dominated, extragalactic radio sources. This makes them suitable candidate reference sources for the next generation (Mk IV/V) astrometry and geodesy reference frames. The increased sensitivity of Mk IV/V VLBI will probably be required to observe the generally lower flux density scintillating sources. While the compact morphology of scintillating sources suggests their use as ICRF sources, their position stability will need to be established.

## 5. CONCLUSIONS

The VLBI observations presented in this paper show that radio sources that exhibit rapid variability in their light curves as a result of radio wave propagation through turbulent electron density fluctuations in the interstellar medium are among the most compact sources in the sky. In particular, the most variable low flux density sources, which constitute the sample observed here, might be the most pointlike and thus, some of the best candidates for densification of the ICRF and consequent improvement in its accuracy. Further, the advent of the Mk IV/V VLBI system, with its greater sensitivity, will make use of weaker sources easier, provided their positional stability can be established.

It is important to note that, as VLBI assumes that sources do not change over the period of observation, the amplitude variability of scintillating sources may introduce spurious structure into their VLBI images and fundamentally limit their fidelity.

We thank Malte Marquarding for writing the AIPS++ scripts used to generate the final contour maps. This research has made use of the United States Naval Observatory Radio Reference Frame Image Database. The VLBA and VLA are facilities of the National Radio Astronomy Observatory, which is operated by Associated Universities, Inc., under a cooperative agreement with the National Science Foundation.

## REFERENCES

Bignall, H. E., et al. 2002, Publ. Astron. Soc. Australia, 19, 29
———. 2003, ApJ, 585, 653
Bridle, A. H., & Greisen, E. W. 1994, AIPS Memo 87
Cotton, W. D. 1993, AJ, 106, 1241
Dennett-Thorpe, J., & de Bruyn, A. G. 2001, Ap&SS, 278, 101
———. 2002, Nature, 415, 57
Fey, A. L., et al. 2004, AJ, 127, 1791
Greisen, E. W. 1988, AIPS Memo 61
Jauncey, D. L., Bignall, H. E., Lovell, J. E. J., Kedziora-Chudczer, L., Tzioumis, A. K., Macquart, J.-P., & Rickett, B. J. 2003a, in ASP Conf. Ser. 300, Radio Astronomy at the Fringe, ed. J. A. Zensus, M. H. Cohen, & E. Ros (San Francisco: ASP), 199
Jauncey, D. L., Johnston, H. M., Bignall, H. E., Lovell, J. E. J., Kedziora-Chudczer, L., Tzioumis, A. K., & Macquart, J.-P. 2003b, Ap&SS, 288, 63
Jauncey, D. L., & Macquart, J.-P. 2001, A&A, 370, L9
Leppänen, K. J., Zensus, J. A., & Diamond, P. J. 1995, AJ, 110, 2479

Lovell, J. E. J., Jauncey, D. L., Bignall, H. E., Kedziora-Chudczer, L., Macquart, J.-P., Rickett, B. J., & Tzioumis, A. K. 2003, AJ, 126, 1699
Ma, C., et al. 1998, AJ, 116, 516
Rickett, B. J. 1990, ARA&A, 28, 561
Rickett, B. J., Witzel, A., Kraus, A., Krichbaum, T. P., & Qian, S. J. 2001, ApJ, 550, L11
Roberts, D. H., Wardle, J. F. C., & Brown, L. F. 1994, ApJ, 427, 718
Schwab, F. R., & Cotton, W. D. 1983, AJ, 88, 688
Shepherd, M. C. 1997, in ASP Conf. Ser. 125, Astronomical Data Analysis Software and Systems VI, ed. G. Hunt & H. E. Payne (San Francisco: ASP), 77
Shepherd, M. C., Pearson, T. J., & Taylor, G. B. 1994, BAAS, 26, 987
Taylor, G. B., & Myers, S. T. 2000, VLBA Scientific Memo 26 (Socorro: NRAO)
Wagner, S. J., & Witzel, A. 1995, ARA&A, 33, 163